Identification of Isothermal crystallization kinetics of poly(ether-ketone-ketone) based on spherulite growth measurements and enthalpic data

Saber Chelaghma, Olivier de Almeida, Philippe Marguerès, Jean-Charles Passieux, Jean-Noël Périé, Alain Vinet, Bénédicte Reine

Identification of Isothermal crystallization kinetics of poly(ether-ketone-ketone) based on spherulite growth measurements and enthalpic data

Saber A. CHELAGHMA
Institut Clément Ader (ICA), Université de Toulouse, CNRS UMR 5312, IMT Mines Albi, INSA, UPS, ISAE, Campus Jarlard, 81013 Albi, France
IRT Saint Exupéry, Toulouse, France

Olivier DE ALMEIDA
Institut Clément Ader (ICA), Université de Toulouse, CNRS UMR 5312, IMT Mines Albi, INSA, UPS, ISAE, Campus Jarlard, 81013 Albi, France

Philippe MARGUERES
Institut Clément Ader (ICA), Université de Toulouse, CNRS UMR 5312, IMT Mines Albi, INSA, UPS, ISAE, 3 rue Caroline Aigle, 31400 Toulouse, France

Jean-Charles PASSIEUX
Institut Clément Ader (ICA), Université de Toulouse, CNRS UMR 5312, IMT Mines Albi, INSA, UPS, ISAE, 3 rue Caroline Aigle, 31400 Toulouse, France

Jean-Noël PERIE
Institut Clément Ader (ICA), Université de Toulouse, CNRS UMR 5312, IMT Mines Albi, INSA, UPS, ISAE, 3 rue Caroline Aigle, 31400 Toulouse, France

Alain VINET
Airbus SAS, Toulouse, France

Bénédicte REINE
IRT Saint Exupéry, Toulouse, France

Dated: June 23, 2020

ABSTRACT: Differential scanning calorimetry and polarized optical microscopy were used in this study to identify the contributions and interactions of both primary and secondary crystallization processes during the isothermal crystallization of a PEKK 70/30. Primary crystallization, which is related to the growth of spherulites, was monitored by polarized optical microscopy. The data collected allowed identifying the corresponding nucleation density and crystal growth rate that were subsequently used to feed a kinetic model derived from Hillier's equation and already been reported in literature. The DSC data were then used to determine the contribution of the secondary crystallization mechanism, considering that primary crystallization is related to the instantaneous nucleation and growth of spherulites. From these data, an inverse approach was used to identify the few remaining parameters of the model. The proposed approach has the advantage of providing kinetic parameters representative of the secondary crystallization mechanism that are not dependent on the inverse identification procedure. Doing so, a non-integer Avrami exponent equal to 2.7 is obtained and discussed.

Keywords: Spherulite nucleation and growth rates; polarized optical microscope; PEKK; Crystallization model identification

INTRODUCTION

In transportation and energy sectors, the current trend is to develop multifunctional competitive composite structures with improved properties (such as thermal and electrical conductivity[1–5]), but also allowing for simplified and cheaper manufacturing processes[6–9] and higher recyclability[10]. In this context, industry and research are moving towards a greater use of semi-crystalline thermoplastic laminates. Currently and mainly because of its outstanding mechanical performances, PEEK (poly(ether ether ketone)) is the most widely used thermoplastic polymer in the aerospace industry. Nevertheless, this resin requires high process temperatures and its cost remains very high. Consequently, new thermoplastic materials are investigated to contribute to further cost reductions for primary aerostructures.

PEKK (poly(ether ketone ketone)), which has been only minimally studied since the 1990s, is notably receiving a renewed interest as an alternative to PEEK. The ratio of ether/ketone entities in PEEK or PEKK macromolecules significantly influences important physical properties. For instance, the melting temperature T_m, the glass transition temperature T_g and the melt viscosity increase with the fraction of ketone entities because of the stiffness of the keto linkages[11,12]. In the case of PEEK, T_g is around 144°C while T_m ranges from 334 to 343°C[13,14]. For its part, PEKK exhibits a higher T_g that ranges from 156°C to 161°C and a greater T_m range, typically from 300°C to 360°C[15]. PEKK properties, like for instance the melting temperature, can thus be modulated via the PEKK formulation.

The particularity of PEKK compared to PEEK is that it is prepared from diphenyl ether (DPE), terephthalic acid (T) and isophthalic acid (I) and different grades can therefore be synthetized regarding the T/I ration[16]. The addition of meta isomers in PEKK significantly reduces its T_m, which offer an advantageous reduction of the processing temperature. However, this also decreases the crystallization rate which can be an issue for the proper control of manufacturing conditions. A better understanding of the relation between the T/I ratio and the crystallization kinetics is then required as well as advanced modeling of PEKK crystallization kinetics[17,18].

Many models have been proposed to describe the crystallization kinetics of semi-crystalline polymers. Among them, Avrami's model[19], that is based on the description of growing

crystalline structures, namely spherulites, is definitely the most used, as well as its extensions to non-isothermal conditions, i.e. Ozawa and Nakamura models[20,21]. Although these models rarely fit the crystallization kinetics over the entire crystallization transition, they allow describing in a simple way the evolution of the relative degree of crystallinity $\alpha(t)$ over time. These models actually turn out to be ill-designed to describe crystallization of PAEKs (poly(aryl ether ketone)s). The Avrami plot of PEKK, that consists in plotting $\ln(-\ln(1-\alpha))$ as a function of $\ln(t)$, is indeed not linear for a PEKK 60/40 T/I ratio[18], with a non-linearity appearing for values of α higher than 0.6. This indicates that crystallization starts in accordance with Avrami's description, but changes by the end of the transformation due to the activation of different crystallization mechanisms. This change is usually referred as secondary crystallization and is related to an interlamellar crystallization process and/or to an improvement of already formed crystals. In the case of PEEK, Verma et al.[22] showed that the secondary crystallization is due to the formation of small crystals of lower melting temperature than that of crystals formed by the first mechanism.

As indicated by the non-linear Avrami plots, a constant Avrami exponent is no longer sufficient for describing PEKK crystallization kinetics. Specific kinetic models have thus been proposed so as to consider the contribution of the secondary mechanism to the overall crystallization process. Velisaris and Seferis[13] and Cebe[14] early proposed kinetic models combining two Avrami equations, each one accounting for each crystallization mechanism. Doing so, they successfully described the isothermal and non-isothermal crystallization kinetics respectively. Later, Bessard[23] proposed to unify the isothermal and non-isothermal models by modifying the thermodependence of model parameters through an Arrhenius law. However, in all these previous approaches, primary and secondary crystallization mechanisms were assumed fully decoupled, even though the description of the secondary mechanism suggest the interdependence of this process with the main primary mechanism. This is Hsiao et al.[17] and recently Tardif et al.[24] and Choupin et al.[18] who re-introduced the coupled kinetic equation originally introduced by Hillier[25] in order to take into account the kinetic coupling of both crystallization mechanisms. This model turned out to be relevant for the modelling of the isothermal crystallization kinetics of a PEKK grade of 60/40 T/I ratio.

Although the introduction of a coupled kinetic equation for modelling PEKK crystal-

lization improves the physical description of the models, all studies are based on enthalpy analyses of Differential Scanning Calorimetry (DSC) measurements and the full set of kinetic parameters are therefore dependent on the identification procedure used. This study then proposes a characterization methodology aiming at reducing the influence of parameter identification for the modelling of PEKK crystallization kinetics. Two complementary monitoring techniques, namely polarized optical microscopy and DSC, were used to identify the contribution of each crystallization mechanism on the overall crystallization process, rather than DSC technique only. The microscopic observation of polymer samples placed under conditions of controlled temperature provided a number of qualitative and quantitative information on the crystallization transformation[26–28]. The optical monitoring allowed for assessing the nucleation and growth steps for the first crystallization mechanism. On the other hand, the classical enthalpic approach based on DSC gave access to the overall transformation involving both mechanisms, and by subtraction of the first mechanism allowed separating the contribution of the secondary mechanism. Based on the experimental results, the isothermal kinetic model first proposed by Hillier[25] and recently applied to PEKK by Choupin et al.[18], has been used to model the crystallization kinetics of a PEKK grade of 70/30 T/I ratio. The primary mechanism has been modeled based on optical measurement data, an inverse approach was developed to identify the constitutive parameters of the secondary crystallization kinetic.

EXPERIMENTAL

Material

A PEKK KEPSTAN 7003 with a 70/30 T/I ratio is studied herein. The polymer was supplied in powder form by ARKEMA. This PEKK presents a T_g of about 162°C and a T_m of about 335°C. In order to facilitate sampling, PEKK films of $40\mu m$ thickness were prepared from the raw powder at 380°C during 3min under a pressure of five bars using a Carver 4386CE press. Thermo-microscopy and DSC experiments presented hereafter were performed on the same batch of material on samples taken from the same films.

Differential Scanning Calorimetry (DSC)

The calorimetric analysis was performed with a power compensated differential scanning calorimeter (DSC) Perkin Elmer 8500 equipped with an Intracooler II under nitrogen. Indium and Zinc were used to calibrate the temperature and heat of fusion prior to experiments. The polymer specimens were taken from the pressed films by using a 5 mm diameter hole punch. The DSC samples were then prepared by sealing two layers of film in hermetic aluminum pans. Doing so, samples with a relatively small amount of PEEK ($4 \pm 0.2mg$) were obtained. The low sample mass allowed minimizing the effect of low thermal conductivity and no correction was thus applied to DSC measurements.

All samples were first heated at 380°C for 5 minutes to erase the thermal history. This temperature is above PEKK equilibrium melting temperature T_m^0 that is reported at around 355°C by Gardner et al. for a PEKK of 70/30 T/I ratio[16]. The exposure time at 380°C was limited to 5 min so as to avoid PEKK degradation before analysis. This procedure allowed considering that the sample crystallization was achieved from a fully amorphous melted polymer.

Crystallization from the melt was performed by cooling the polymer specimen at 150°C/min to an isothermal crystallization temperature. The high cooling rate used allowed considering that crystallization only occurred after the beginning of the isothermal stage even for relatively low crystallization temperatures. After completion of crystallization, the samples were cooled back to room temperature at 150°C/min.

Polarized optical microscopy

Thermo-microscopic analyses were carried out using a Linkam THMS 600 hot stage coupled with a polarized optical microscope from Huvitz. This equipment, calibrated shortly before the test runs by Linkam, has a thermal stability of less than 0.1°C over a broad range of working temperature (as reported in the calibration certificate).

The microscopic observations were performed in transmission mode on one single layer of the 40μm thick PEKK films lain on a clean glass coverslip of 16 mm diameter. Similarly to DSC experiments, the samples were first heated for 5 minutes at 380°C so as to start the

crystallization procedure from a free-nuclei melt ($T_m^0 \simeq 355°C$ according to Gardner et al.[16]) and then cooled to the isotherm temperature at 150°C/min. Image sequences of isothermal crystallization were recorded for temperatures ranging from 270°C to 315°C.

Here again, the high cooling rate applied for reaching the isotherm temperature was assumed not having an influence on the crystallization process. As discussed hereafter, although the monitoring of the crystalline structures was performed over the entire thermal cycle, measurements of their number and growth was quantified several tens of seconds after the beginning of isotherm, when the hot stage temperature is stabilized. It was thus considered that the stabilization of the sample temperature at the beginning of the isotherm phase had only a limited influence on the crystallization of PEKK, and in particular on the formation of stable nuclei.

In addition to the isothermal study, non-isothermal crystallization conditions were also investigated in order to analyze the growth rate of the crystal structures under higher supercooling conditions. The non-isothermal crystallization of PEKK from the molten state was carried out at different cooling rates ranging from 5 to 100°C/min. The thermal offset when increasing the cooling rate has not been corrected although it may have affected the temperature to which the results were reported. This was decided because the data recorded in non-isothermal conditions were combined with the isothermal data and therefore have a very limited effect on the identification of the associated kinetic parameter.

Thanks to the difference of optical indices of the crystalline and amorphous phases, PEKK crystallization process could be observed under polarized optical microscope by following the growth of crystalline lamellas and the formation of spherulites within the amorphous phase (Figure 1(left)). The spherulitic microstructure appeared even more distinctly by placing the sample in the optical microscope between crossed polarizer and analyzer (Figure 1(right)). The alignment of the polymer molecules within the lamellas results in birefringence producing a variety of colored patterns, including a Maltese cross[29]. In practice, the position of the axes of the two polarizing filters was optimized so as to obtain the best contrast between the spherulites and the melted amorphous phase around them. This way, it was possible to monitor the crystallization process and to quantify the number and the growth rate of the spherulites. Images recorded using a magnification of x100 (small enough to study a

representative amount of matrix) were used to quantify the number and growth rate of crystalline structures.

EXPERIMENTAL RESULTS

Analysis of calorimetry data

The Figure 2 presents the heat flow change recorded during the isothermal crystallization of PEKK 70/30 from the metastable melt at different isotherm temperatures. The investigated crystallization temperatures in DSC were limited to the range from 270°C to 290°C. Indeed, at high temperature, crystallization lasts for tens of minutes and the crystallization peak spreads over a large period of time. The identification of the crystallization enthalpy by defining a baseline on DSC traces then becomes imprecise. Conversely, at low temperature, crystallization is so fast that the stabilization of the DSC signal at the beginning of the isotherm is superimposed with the exothermic peak which induces uncertainty on the measured enthalpy.

As systematically reported in the literature, the starting point of isothermal crystallization cannot be clearly identified when using a conventional DSC. Crystallization usually starts during the stabilization of the signal between the cooling and isothermal phases which generates a high uncertainty on the assessment of the start of crystallization exotherm. Depending on the study, with reference to the linear baseline which is clearly drawn after the end of crystallization, the peak of exothermic crystallization can be or truncated, i.e. no interception of the heat flow curve with the horizontal baseline, or it can start at a higher heat flow level than the baseline level. Two main strategies are thus applied in order to overcome these issues. In the first case, the classical procedure consists in a backward extrapolation of the crystallization peak slope in order to get an intersection point with the horizontal baseline[18]. In the second case, that was encountered by Hsiao et al. or Tan et al.[17,30], the strategy consist in assuming the intersection point between the heat flow curve and the baseline as the starting point.

In the present case, by limiting the range of studied temperatures, the backward extrapolation of the DSC baseline was intercepting the heat flow signal at its maximum value for

all crystallization temperatures between 290°C and 275°C (Figure 3). It was thus assumed that the DSC signal was stabilized before the start of crystallization and no assumption was thus required for the definition of the heat flow baseline and for the crystallization peak integration. For the integration of the crystallization heat flow recorded at 270°C, the same procedure used by Choupin et al.[18] was applied. Nevertheless, as presented by Tardif et al.[24], a phase change go with a variation of the specific heat resulting in an inflection of the crystallization exotherm baseline on the DSC signal, and an uncertainty remains about the validity of this point as a baseline reference of crystallization exotherm.

The relative extent of crystallinity which developed at time t, $\alpha(t)$, was then determined by integration of the exotherms using equation 1, in which $Q(t)$ is the heat flow at time t due to crystallization, and $\int_0^{t_\infty} Q(t)dt$ is the total area of the crystallization peak. The resulting crystallization kinetics of PEKK 70/30 are plotted in Figure 3 for the different crystallization temperatures.

$$\alpha(t) \; = \; \frac{\int_0^t Q(t)dt}{\int_0^\infty Q(t)dt} \tag{1}$$

A shown in Figure. 3, the curves of relative crystallinity exhibit a non-symmetrical sigmoidal. In particular, for the lowest temperatures (290°C), the last 20% of the crystallization process represent about 30% of the crystallization time. This absence of symmetry is attributed to the existence of a secondary crystallization mechanism that occur in parallel with the nucleation and growth of lamellas within the spherulites, as already reported for various of the Poly-Aryl-Ether-Ketone family by several authors[13,17,18,22,31].

This is confirmed by the Avrami plot shown in Figure 4. This plot of the $ln(-ln(1-\alpha(t))$ vs. $ln(t)$ that is based on Avrami's equation is not linear on the entire duration of crystallization and therefore confirms the limitation of Avrami's model to predict the crystallization kinetics of PEKK with accuracy.

Analysis of microscopic data : nucleation density

The ImageJ Particle Analysis module was used to count the number of crystalline structures in a given image and a threshold of 20 pixels was taken into account in order to distinguish growing structures from the background noise (Figure 5). The use of a threshold was required because the location where nuclei are formed affects the contrast of spherulites' boundary.

Spherulites initiated close to the top surface have a contrasted boundary that facilitates their identification. Conversely, spherulites formed close to the glass plate surface are observed though the melt and they can only be distinguished from the background noise when bigger. This can be observed in Figure 8: some spherulites are barely visible while others are well contrasted. The value of 20 pixels as a threshold for the numbering of spherulites was found as the best compromise. A lower value increased the uncertainty of particles' numbering due to the confusion of less contrasted spherulites with the background noise, and a higher value did not allow separating adjacent spherulites before impingement.

By following this procedure, the smallest identified particles and having been taken into account had a diameter of approximately 2 μm, which is far bigger than the size of a stable nucleus[32]. However, the homogeneous distribution of the small spherulites on the image and the distance between them makes it possible to consider that each spherulite was formed from a single nucleus although the probability of two nuclei generated very close to each other cannot be ruled out.

Besides, the observation of spherulites of different contrasts but of similar diameter gave confidence in the low influence of surfaces (free surface and glass plate surface) on the nucleation process. It was thus assumed that the measurements of nucleation density are representative of the bulk nucleation of PEKK 70/30. Moreover, as the DSC samples were twice thicker than the microscopy specimens (two layers of PEKK film instead of one), it was considered that the nucleation process was similar in both experiments.

In the hot stage, an instantaneous nucleation was observed for each isothermal crystallization condition. As shown in Figure 6, the number of nuclei increases when the isothermal temperature decreases. Thanks to the particle analysis module of ImageJ, the number of nuclei for each isothermal temperature could be quantified. The Figure 7 presents the evolution of the nucleation number with respect to the isotherm temperature.

Although it was possible to obtain qualitative information on crystallization over a large range of temperatures, the nucleation density could not be assessed below 270°C. Its increase when decreasing the crystallization temperature made the nuclei numbering imprecise below this temperature. In the same way, under non-isothermal conditions, the number of nuclei increased over time with the decrease of the temperature. New nuclei regularly appeared

between growing spherulites and the determination of the nucleation density was uncertain. Thus the nucleation numbering was not performed on non-isothermal data.

Analysis of microscopic data : growth rate

The growth rate was measured from the radius evolution of several spherulites that were well contrasted. To do so, for each snapshot of the image sequence until impingement of spherulites, a column of pixels along the diameter of a spherulite was collected. The pixel stripes were then all stacked horizontally so as to build a diameter-time diagram (Figure 8). One pixel in the horizontal dimension represents the time period of the acquisition framerate, the vertical axis displays the diameter of a spherulite. The outline of the diameter-time plot was used to estimate the time evolution of spherulite radius, and thus, to quantify the growth rate.

Figure 8 shows that under isothermal conditions, the size of the spherulites evolves linearly with time and that the crystal growth rate is therefore constant. As a result, the growth rate V could simply be estimated from the tangent of the angle γ between the dashed yellow line indicated in Figure 8 and the horizontal axis using equation 2 in which δ is the image resolution (mm/pix) and I is the acquisition framerate (s^{-1}), here $I = 1$ image per second.

$$V = \tan\gamma \;\; \delta \, I \tag{2}$$

As already mentioned, the rate of spherulite growth has been found to be constant for any isothermal stage. It tends, like the nucleation density, to increase when the temperature decreases (Figure 9). It varies from 1 to 10μm/min when the temperature goes from 315 and 270°C. Thus the acceleration of crystallization kinetics observed by DSC as the isothermal temperature decreases can be attributed to an increase of both the nucleation density and the crystal growth rate.

Unlike the isothermal case, the growth rate is not constant in non-isothermal conditions. However, considering that the growth rate is only temperature dependent, its evolution could be assessed during non-isothermal crystallization using the same procedure as for isothermal crystallization. To do so, the diameter-time diagram in Figure 8 was build at different times of the cooling phase with sequences of a few successive images. Several growth rates were

therefore identified over the range of temperature of non-isothermal crystallization.

The measurements performed on data collected at different cooling rates are presented in Figure 9. A good agreement appears between the non-isothermal and isothermal growth rates insofar as the slight difference between the two data sets can be attributed to the inertia of the heating device. This suggest that the assumption of a growth rate independent on the cooling rate and only depends on the temperature is valid, and that the development of a unified model describing the growth rate both for isothermal level and different cooling rates is possible.

The combination of isothermal and non-isothermal growth rates in Figure 9 exhibits a bell-shaped curve that is in good agreement with Lauritzen and Hoffman's theory[33]. Near the glass transition temperature, the growth of crystallites is limited by low molecular motion that stops chains diffusion (high viscosity of the molten phase). At high temperature, close to the melting temperature, the formation of thermodynamically stable nucleus is unfavorable which consequence is a low crystal growth rate[33].

Crystallization time

Apart from the determination of nucleation and spherulite growth rates, the image sequences recorded during the isothermal crystallization of PEKK 70/30 under microscope can provide additional informations about the crystallization phase change. For instance, Ding and Spruiel[34] demonstrated that the transmitted light intensity is an indicator of the crystallization kinetics, although it was shown that the light depolarization technique could not be used a conventional measure of the degree of crystallinity, quantitatively comparable with calorimetric, density or X-ray diffraction data[35].

In the present study, the image sequence from microscopic observations was simply used to determine a crystallization time representative of nucleation and growth process.For that purpose, the image area covered with spherulites was quantified on each image of the sequence after binarization. The crystallization time was then simply associated to the image for which the surface covered by the spherulites no longer developed. The resulting crystallization time is compared in Figure 10 with the crystallization time identified on DSC curves. This latter value of crystallization time was taken for a relative crystallinity of 99% (Figure 3).

The Figure 10 revealed that the time required for the spherulites to fill the image field was shorter than the crystallization time obtained from DSC experiments. Of course, this difference can be partially attributed to the method used to determine the crystallization time from microscopic observations. The binarization of the sequence of images supposes the projection of 3D phenomena in a 2D plane. The crystallization time determined by this method therefore does not accurately reflect the time needed by the spherulites to entirely fill the volume of the sample. In particular, spherulite's impingement occurring though the thickness of the sample is hidden, inducing as a consequence an underestimation of the actual crystallization time. The difference of crystallization time is however significant, the time for PEKK isothermal crystallization under microscope being twice as short as the crystallization time taken from DSC data, which can not be only induced by the method used.

As well as the non-symmetrical shape of relative crystallization sigmoids, the difference in crystallization time is related to the existence of two crystallization mechanisms occurring during PEKK crystallization. However, even if they occur simultaneously over a part of the transformation, the two phenomena are sequenced and the secondary crystallization seems to be the mechanism that ends the overall crystallization transformation. Conversely, spherulitic nucleation and growth can legitimately be considered as the first process activated within the molten medium.

MODELING APPROACH

Hillier's crystallization model

As previously detailed, several models have been proposed in literature to describe the isothermal crystallization kinetics of PAEKs. Among the various attempts to integrate both primary and secondary crystallizations in the kinetic modeling of crystallization, perhaps the most relevant approach is the model proposed by Hillier in 1965[25]. In this model, the crystallization at time t is expressed in an identical way as in other models taking into account the contribution of two crystallization mechanisms with equation 3, where $\alpha_i(t)$ and $w_i(t)$ are the relative crystallinity and the proportion of each mechanism, the index i being equal to 1 for primary crystallization and 2 for the secondary crystallization, with $w1 + w2 = 1$

indicating that the total relative crystallinity at infinite time is unity.

$$\alpha(t) = \sum w_i \, \alpha_i(t) \tag{3}$$

In equation 3, the relative crystallinity $\alpha_1(t)$ is modeled by an Avrami equation (equation 4), where K_1 is the rate constant of crystallization and n_1 is the Avrami exponent.

$$\alpha_1(t) = 1 - \exp(-K_1 t^{n_1}) \tag{4}$$

The originality of Hillier's formalism lies in the description of the secondary crystallization kinetics $\alpha_2(t)$. The secondary crystallization mechanism is assumed to occur according to an Avrami equation $\beta_2(t)$ (equation 5), with a crystallization rate K_2 and an Avrami exponent n_2. However, the kinetic of this second process is assumed constrained by the advancement of primary crystallization according to equation 6. It must be noticed that the Avrami exponent n_2 of the secondary crystallization was set to 1 in the original version of the model proposed by Hillier in 1965[25].

$$\beta_2(t) = 1 - \exp\left(-K_2(t)^{n_2}\right) \tag{5}$$

$$\alpha_2(t) = \int_0^t \alpha_1(\theta) \frac{d\beta_2(t-\theta)}{dt} d\theta \tag{6}$$

This assumption of the dependance of the secondary crystallization mechanism upon the avancement of the first one then gives a total relative crystallinity according to equation 7.

$$\alpha(t) = w_1 \, \alpha_1(t) - (1 - w_1) \int_0^t \alpha_1(\theta) \times K_2 n_2 (t-\theta)^{n_2 - 1} \times \left(1 - \exp\left(-K_2(t-\theta)^{n_2}\right) d\theta \right. \tag{7}$$

Modeling strategy

By using that model, Hsiao et al.[17], Choupin et al.[18] and Tardif et al.[24] could predict PEKK isothermal crystallization kinetics with accuracy and separate the contributions of primary and secondary crystallization mechanism on the overall crystallization process. In addition they could show that the activation of the secondary crystallization was delayed as regards to primary crystallization, which is consistent with our analysis of the crystallization time.

This model was thus selected for the modeling of PEKK 70/30 isothermal crystallization kinetics.

The identification of the constitutive parameters of kinetic models involving two mechanisms has however always been based on enthalpic measurements without taking into account experimental data of spherulitic growth[13,17,18,22,24,31,36]. Choupin et al.[18] well observed spherulite growth under polarized microscope but limited the use of those experimental data along with the slope of the Avrami plot to the definition of the Avrami exponent of primary crystallization. Nevertheless, doing so, they clearly considered for the first time that primary crystallization, as defined in Hillier's formalism, is related to the nucleation and growth of spherulites which was not clearly stated in previous literature.

That statement is also used herein for the modeling of PEKK isothermal crystallization kinetics, but in order to properly account for nucleation and growth processes, thermo-microscopic measurements have been exploited in addition to more conventional DSC measurements to identify the constitutive parameters of Hillier's model. The nucleation density and growth rate were used to identify the kinetics of the primary crystallization mechanism while enthalpic data were used to determine the secondary mechanism kinetics. This approach limits the influence of numerical artefacts induced by the inverse identification of coupled parameters.

Kinetic parameters of primary crystallization

Following the general approach reported in literature for nucleation and crystallization growth[37], Avrami's constants can be expressed as a function of the initial number of nuclei (N) and the crystal growth rate (G) depending on the dimensionality of crystal growth and the nucleation mode. For the primary crystallization, a spherulitic growth with an instantaneous nucleation was observed under microscope for PEKK. Therefore, the Avrami exponent n_1 was set to 3 considering the three-dimensional growth of spherulite structures. This value is by the way consistent with the linear section of the curves in the Avrami plot (Figure 4). The linear sections of those curves exhibit a slope of 2.7, and 3 is thus the closest integer. It can be noted that the value of n_1 identified for a PEKK 70/30 T/I ratio is higher than the one identified by Choupin et al.[18] for a PEKK 60/40. The crystallization rate constant

K_1 could finally be expressed according to equation 8. The rate constant K_1 was thus only defined from the experimental values of the nucleation density N and growth rate G.

$$K_1 = \frac{\pi}{3} G^3 N \tag{8}$$

Several authors, including Angelloz et al.[38] and Koscher et al.[39], have shown a logarithmic evolution of the thermally activated nuclei as a function of the degree of supercooling ΔT ($\Delta T = T_m^0 - T$, with T_m^0=355°C the equilibrium melting temperature taken from Gardner et al.[16]). In equation 9, a and b are material dependent parameters and N the nucleation density.

$$N = \exp\big(a(T_{m0} - T) + b\big), \tag{9}$$

Unlike in[38] where the parameters of such a model were determined experimentally by DSC, it was, here, identified using the thermo-microscopy data. As shown in Figure 7, the model proposed by Koscher et al.[39] described with a suitable accuracy the evolution of the nucleation density for all isotherm temperatures throughout the investigated range of temperature.

In this work, Lauritzen-Hoffman model was selected to describe the spherulite growth rate in PEKK resin. According to the Hoffman and Lauritzen theory[33], the radial growth rate of spherulites can be expressed as in equation 10.

$$G_i(T) = G_{0i}\ \exp\left(-\frac{U^\star}{R(T - T_\infty)}\right) \exp\left(-\frac{K_{gi}}{T\Delta T f}\right) \tag{10}$$

In equation 10, G_{0i} is a pre-exponential factor independent of temperature. In the first exponential term that is related to the contribution of the diffusion process to the growth rate, $U^\star$ is the activation barrier to transport molecules from the melt to the crystal surface ($U^\star = 6300 J/mol$[33]) , T_∞ is the temperature at which viscous flow ceases ($T_\infty = T_g - 30$K, with $T_g = 160$°C) and R is the universal gas constant ($R = 8.314 J/K/mol$). In the second exponential term which corresponds to the contribution of the nucleation process, K_{gi} is the activation energy of nucleation for a crystal with a critical size and the term f is a correction factor to account for temperature dependence of enthalpy of fusion with temperature and

is denoted by $f = 2T/(T_{m0} + T)$. Figure 9 presents the measured and simulated crystal growth rates as a function of the crystallization temperature. Both data are in excellent agreement throughout the range of investigated temperatures, which confirms the relevance of the Lauritzen-Hoffman model for PEKK.

Identification of overall crystallization kinetics

The kinetic curves obtained from DSC were then used to identify the Avrami exponent n_2 and the crystallization rate constant K_2 of the second mechanism, along with the weight factor w_1. The Avrami exponent n_2 was kept constant while K_2 and w_1 (and consequently w_2) were considered as temperature dependent. All parameters of the crystallization model where identified to minimize the gap between the model and the experimental data in a least-squares sense. The arising non-linear least-square problems were efficiently solved using the Levenberg-Marquardt algorithm.

For all the studied isotherm temperatures, the time evolution of the overall relative crystallinity of PEKK 70/30 measured by DSC is correctly simulated by using the identified Hillier model. As depicted in Figure 11, the crystallization can remarkably be separated into two distinct processes. At the beginning, the crystallization process is well described by the sole nucleation and growth parameters, which confirms primary crystallization is directly related to the nucleation and growth of spherulites. For all crystallization temperatures, the secondary process is delayed and starts after about 20% of total relative crystallization. This demonstrates that the secondary crystallization mechanism requires a minimum level of conversion for being activated.

Table 1 provides, for each model parameter, the data used for their identification and the corresponding optimal value. The temperature dependency of K_2 and w_2 parameters is shown in Figure 12.

DISCUSSION

As depicted by the evolution of w_1 with temperature, the primary process contribution is highly temperature dependent with a proportion changing from 92% at 270°C down to 57%

Mechanism	Parameter		Value	Identification
1	Avrami exponent	n_1	3	fixed
1	Nucleation parameters	a [K^{-1}]	0.0638	hot stage
1		b	25.2	hot stage
1	Growth rate parameters	G_{0i} [$\mu m.s^{-1}$]	0.501	hot stage
1		K_{gi} [K^2]	680.10^3	hot stage
2	Avrami exponent	n_2	2.7	DSC
2	Rate constant	K_2 [s^{-n_2}]	(see Figure 12)	DSC
1 and 2	Balance of mechanisms 1 and 2	w_1	(see Figure 12)	DSC

Table 1: Identification of the parameters of the crystallization model.

at 290°C. This proportion of primary crystallization decreases as the temperature increases in a similar manner as for the nucleation density and spherulite growth rate in this range of temperature. A dominating primary crystallization then seems correlated with the formation of numerous small spherulites. Reciprocally, the secondary crystallization process may require large spherulites to occur in large proportion. The fractionation and segregation of low molecular weight molecules during the lamellar growth could be one of the reasons of such change in the crystallization process[26]. This could be investigated further by analyzing the influence of the addition of low molecular weight PEKK on the crystallization transformation and in particular on the proportion of the secondary crystallization mechanism. The decrease of the kinetic constant K_2 with the increase of temperature indicates that the secondary mechanism is also highly temperature dependent. The large spherulites along with a slow growth rate may thus be required for a significant contribution of the secondary crystallization to to total crystallization process.

Parameter identification led to a non-integer value of the Avrami exponent n_2 related to the secondary crystallization. This value is higher than the values reported in literature for this secondary mechanism. Indeed, Hsiao et al.[17], who also used Hillier's equation for modeling PEKK isothermal crystallization kinetics arbitrary used integer values for the Avrami exponents n_1 and n_2, 4 and 2 respectively. The choice of those parameters was based on results of previous studies in which the crystallization behavior was modeled with a different

kinetic equation. For their part, Choupin et al.[18], who also used Hillier's equation, did not assume the exponents of primary and secondary crystallization mechanisms from literature but set their value based on their own experimental data. The Avrami exponent of the primary crystallization was selected as the closest integer to the slope of the linear section in the Avrami plot, and found $n_1 = 2$. Then they set the second exponent n_2 equal to unity, as it led to the best results of fitting and considering that the secondary mechanism is related to an integer exponent value. A similar strategy was applied by Tardif et al.[24]. By using a nano-DSC, they could explore the crystallization behavior over a broad range of crystallization temperature. They identified $n_1 = 3$ from the crystallization half-time curves but did not assume a constant n_2. They identified that n_2 is equal to 2 for temperatures below 260°C and is equal to 1 for temperatures above 260°C.

By selecting an integer value of the Avrami exponents for modeling the secondary crystallization kinetics, previous authors indirectly assumed that PEKK crystallization process results from only two crystallization mechanism. The value of 2.7 however suggests that the secondary crystallization mechanism is not related to a unique process but to the formation of crystalline structures of different dimensions that can be 2D (fibrillar) or 3D (lamellae). The thickening of lamellae formed during primary crystallization could also be a possible secondary process (1D growth).

This assumption of multiple mechanisms involved in the secondary crystallization only relies on a non-integer value of the Avrami exponent. However, this can be raised thanks to the limited number of constitutive model parameters that were identified numerically. In particular, the uncertainty related to the stabilization of the DSC signal at the early stage of isothermal crystallization could be limited by the direct interpretation of microscopic data. As presented by Tardif et al.[24], a phase change go with a variation of the specific heat resulting in an inflection of the crystallization exotherm baseline on the DSC signal. None of the procedures proposed in literature are therefore valid for an accurate assessment of isothermal crystallization exotherm. Nevertheless, this section of crystallization curves is of prime importance for the identification of model parameters. It actually becomes critical when it is assumed that two distinctly different Avrami type crystallizations are operative during the transformation, as the choice of the first exponent affects the determination

of the secondary crystallization kinetic parameters. For instance, Choupin et al.[40] set an Avrami exponent n_1 to a value of 2 for primary crystallization, although they admit that the observation of instantaneous apparition of spherulites was better relying on a value of 3 for n_1. This value of 2 was chosen as it corresponded to the closest integer to the slope in the Avrami plot, but also because this value allowed rebuilding the beginning of the crystallization exotherm with a linear backward extrapolation of the heat flow slope. This choice nonetheless introduced an induction time that had to be identified but may have also influenced the identification of the other parameters.

Finally, the approach proposed here for model identification, which is based on the combination of two sets of experimental data, provides new insights into the secondary crystallization process. Further investigation on both the crystallization microstructure and kinetic parameters should be performed on the results of secondary kinetics. The analysis of crystallization regimes, as described by Lauritzen et al.[41] and recently applied by Seo et al.[36], could give a better understanding of both the primary and secondary crystallization mechanisms.

CONCLUSIONS

A characterization of the isothermal crystallization of a PEKK 70/30 using polarized optical microscopy and differential scanning calorimetry is presented. A Hillier model was selected to describe the whole crystallization process considering that the primary process is directly related to the nucleation and growth of spherulites. An original identification procedure data was then developed. The constitutive parameters associated with the primary crystallization mechanism were determined solely using thermo-microscopy data, while the remaining parameters (the constitutive parameters associated with the second mechanism and the relative weight factor of the mechanisms in the whole crystallization process) were finally identified thanks to DSC data. A good correlation with the experimental data has been obtained for all the studied isothermal conditions, and the results showed that the secondary crystallization mechanisms may not be only related to a unique process but to multiple mechanisms of various dimensions. Finally, it should be noted that the original use of this experimental data set brings a certain robustness to the identification procedure by limiting the number

of parameters of the kinetic model to be identified by the inverse method.

In further studies, the experimental protocoles should be improved so as to explore a broader range of temperature and confirm the conclusions raised in this study. The crystallization regimes should also be investigated further so correlate the kinetic parameters with energetic factors. On the other hand, for the modeling of composite manufacturing, the influence of fibers should be taken into account and in particular, the nucleation and growth process on fibre surface should be analyzed. Specific and efficient computational techniques are also needed to simulate the crystallization in large composite parts. Some of these points have already been addressed and will be the subject of separate articles.

ACKNOWLEDGMENTS

The results of this study were obtained in the context of the research project "COMPINNOVTP" at the IRT Saint Exupéry. We thank the industrial members who supported this project through their contributions, both financial and in terms of specific knowledge: Airbus SAS, Airbus Operations, Ariane Group, Airbus Helicopters and Thales Alenia Space. We also thank the "Commissariat Général aux Investissements" and the "Agence Nationale de la Recherche" for their financial support in the framework of the "Programme d'Investissement d'Avenir" (PIA).

References

1. R. Hollertz, S. Chatterjee, H. Gutmann, T. Geiger, F. A. Nüesch, and B. T. T. Chu, Nanotechnology **22**, 125702 (2011).

2. E. Kandare, A. A. Khatibi, S. Yoo, R. Wang, J. Ma, P. Olivier, N. Gleizes, and C. H. Wang, Composites Part A: Applied Science and Manufacturing **69**, 72 (2015), ISSN 1359-835X, URL http://www.sciencedirect.com/science/article/pii/S1359835X14003364.

3. R. Moriche, M. Sánchez, A. Jiménez-Suárez, S. Prolongo, and A. Ureña, Composites Part B: Engineering **98**, 49 (2016), ISSN 1359-8368, URL http://www.sciencedirect.com/science/article/pii/S1359836816305686.

4. Y. Lin, M. Gigliotti, M. C. Lafarie-Frenot, J. Bai, D. Marchand, and D. Mellier, Composites Part B: Engineering **76**, 31 (2015), ISSN 1359-8368, URL http://www.sciencedirect.com/science/article/pii/S1359836815001018.

5. K. Hamdi, Z. Aboura, W. Harizi, and K. Khellil, Journal of Composite Materials **52**, 1495 (2018), https://doi.org/10.1177/0021998317726588, URL https://doi.org/10.1177/0021998317726588.

6. A. R. Offringa, Composites Part A: Applied Science and Manufacturing **27**, 329 (1996), ISSN 1359-835X, 4th International Conference on Automated Composites, URL http://www.sciencedirect.com/science/article/pii/1359835X95000487.

7. C. Ageorges, L. Ye, and M. Hou, Composites Part A: Applied Science and Manufacturing **32**, 839 (2001), ISSN 1359-835X, URL http://www.sciencedirect.com/science/article/pii/S1359835X00001664.

8. A. Yousefpour, M. Hojjati, and J.-P. Immarigeon, Journal of Thermoplastic Composite Materials **17**, 303 (2004), https://doi.org/10.1177/0892705704045187, URL https://doi.org/10.1177/0892705704045187.

9. U. K. Vaidya and K. K. Chawla, International Materials Reviews **53**, 185 (2008), https://doi.org/10.1179/174328008X325223, URL https://doi.org/10.1179/174328008X325223.

10. G. Oliveux, L. O. Dandy, and G. A. Leeke, Progress in Materials Science **72**, 61 (2015), ISSN 0079-6425, URL http://www.sciencedirect.com/science/article/pii/S0079642515000316.

11. J. P. Jog and V. M. Nadkarnit, Journal of Applied Polymer Science **32**, 3317 (1986), https://onlinelibrary.wiley.com/doi/pdf/10.1002/app.1986.070320133, URL https://onlinelibrary.wiley.com/doi/abs/10.1002/app.1986.070320133.

12. R. J. Abraham and I. S. Haworth, Polymer **32**, 121 (1991), ISSN 0032-3861, URL http://www.sciencedirect.com/science/article/pii/003238619190571Y.

13. C. N. Velisaris and J. C. Seferis, Polymer Engineering & Science **26**, 1574 (1986), URL https://www.onlinelibrary.wiley.com/doi/abs/10.1002/pen.760262208.

14. P. Cebe and S.-D. Hong, Polymer **27**, 1183 (1986), ISSN 0032-3861.

15. L. Q. Cortes, A. Lonjon, E. Dantras, and C. Lacabanne, Journal of Non-Crystalline Solids **391**, 106 (2014), ISSN 0022-3093.

16. K. H. Gardner, B. S. Hsiao, R. R. Matheson, and B. A. Wood, Polymer **33**, 2483 (1992), ISSN 0032-3861.

17. B. S. Hsiao, I. Y. Chang, and B. B. Sauer, Polymer **32**, 2799 (1991), ISSN 0032-3861.

18. T. Choupin, B. Fayolle, G. Régnier, C. Paris, J. Cinquin, and B. Brulé, Polymer **111**, 73 (2017), ISSN 0032-3861.

19. M. Avrami, The Journal of Chemical Physics **9**, 177 (1941), ISSN 00219606, https://doi.org/10.1063/1.1750872, URL https://doi.org/10.1063/1.1750872.

20. T. Ozawa, Polymer **12**, 150 (1971), ISSN 0032-3861, URL http://www.sciencedirect.com/science/article/pii/0032386171900413.

21. K. Nakamura, T. Watanabe, K. Katayama, and T. Amano, Journal of Applied Polymer Science **16**, 1077 (1972), URL https://onlinelibrary.wiley.com/doi/abs/10.1002/app.1972.070160503.

22. R. Verma, H. Marand, and B. Hsiao, Macromolecules **29**, 7767 (1996), ISSN 0024-9297.

23. E. Bessard, O. De Almeida, and G. Bernhart, Journal of Thermal Analysis and Calorimetry **115**, p. 1669 (2014), URL https://hal.archives-ouvertes.fr/hal-01611997.

24. X. Tardif, B. Pignon, N. Boyard, J. W. Schmelzer, V. Sobotka, D. Delaunay, and C. Schick, Polym. Test. **36**, 10 (2014), ISSN 01429418, URL http://dx.doi.org/10.1016/j.polymertesting.2014.03.013.

25. I. H. Hillier, Journal of Polymer Science Part A: General Papers **3**, 3067 (1965), https://onlinelibrary.wiley.com/doi/pdf/10.1002/pol.1965.100030902, URL https://onlinelibrary.wiley.com/doi/abs/10.1002/pol.1965.100030902.

26. H. D. Keith and F. J. Padden Jr., Journal of Applied Physics **35**, 1270 (1964).

27. J. Varga, J. Mater. Sci. pp. 2557–2579 (1992), ISSN 00222461, URL https://doi.org/10.1007/BF00540671.

28. L. Freire, C. Combeaud, G. Monge, N. Billon, and J.-M. Haudin, POLYMER CRYSTALLIZATION **2**, e10028 (2019), https://onlinelibrary.wiley.com/doi/pdf/10.1002/pcr2.10028, URL https://onlinelibrary.wiley.com/doi/abs/10.1002/pcr2.10028.

29. L. Gránásy, T. Pusztai, G. Tegze, J. A. Warren, and J. F. Douglas, Physical Review E **72**, 011605 (2005).

30. S. Tan, A. Su, J. Luo, and E. Zhou, Polymer (Guildf). **40**, 1223 (1999), ISSN 00323861.

31. P. Cebe, Polymer Engineering and Science **28**, 1192 (1988), ISSN 0032-3888, URL http://doi.wiley.com/10.1002/pen.760281809.

32. C. Li and A. Strachan, Polymer (Guildf). **174**, 25 (2019), ISSN 00323861, URL https://doi.org/10.1016/j.polymer.2019.04.053.

33. J. Hoffman and J. Lauritzen, Journal of Research of the National Bureau of Standards **65**, 297 (1961), URL https://doi.org/10.6028/jres.065A.035.

34. Z. Ding and J. E. Spruiell, J. Polym. Sci. Part B Polym. Phys. **34**, 2783 (1996), ISSN 08876266.

35. A. Ziabicki and B. Misztal-Faraj, Polymer (Guildf). **46**, 2395 (2005), ISSN 00323861.

36. J. Seo, A. M. Gohn, O. Dubin, H. Takahashi, H. Hasegawa, R. Sato, A. M. Rhoades, R. P. Schaake, and R. H. Colby, Polym. Cryst. **2** (2019), ISSN 2573-7619.

37. L. Mandelkern, *Crystallization kinetics of homopolymers: bulk crystallization* (Cambridge University Press, 2004), vol. 2, p. 1–214, 2nd ed.

38. C. Angelloz, R. Fulchiron, A. Douillard, B. Chabert, R. Fillit, A. Vautrin, and L. David, Macromolecules **33**, 4138 (2000), ISSN 00249297.

39. E. Koscher and R. Fulchiron, Polymer **43**, 6931 (2002), ISSN 00323861.

40. T. Choupin, B. Fayolle, G. Régnier, C. Paris, J. Cinquin, and B. Brulé, Polymer (Guildf). **155**, 109 (2018), ISSN 00323861, URL https://doi.org/10.1016/j.polymer.2018.08.060.

41. J. Lauritzen Jr. and J. Hoffman, Journal of Applied Physics **44**, 4340 (1973), cited By 588, URL https://aip.scitation.org/doi/10.1063/1.1661962.

Figure 1: Crystal morphology of PEKK : (left) Lamellae inside spherulites and (right) Maltese cross on spherulites.

Figure 2: Crystallization exotherms of PEKK 70/30 during isothermal crystallization from the melt.

Figure 3: crystallization kinetics of PEKK 70/30 for different isothermal stages.

Figure 4: Avrami plot for PEKK 70/30 isothermally crystallized in a DSC between 270°C and 290°C.

Figure 5: Particles identification in a micrograph thanks to the "particle analysis" module of ImageJ using a threshold of 20 pixels: original image (left) and analyzed image (right).

Figure 6: Small spherulites formed in a neat PEKK resin during an isothermal crystallization at 315°C (top left), 300°C (top right) and 280°C (bottom).

Figure 7: Nucleation density in a neat PEKK resin as a function of isothermal crystallization temperature. Comparison of the simulated and the measured nucleation density for a PEKK 70/30.

Figure 8: Thermo-microscopy analysis: (top) crystallization of a PEKK 70/30 at 290°C revealed by polarized optical microscopy for three different snapshots (after 75s, 224s and 355s) and (bottom) temporal evolution of the diameter of a spherulite as a function of time.

Figure 9: Spherulite growth rate in a PEKK 70/30 resin as a function of isothermal crystallization temperature. The red squares and black circles are experimental data recorded under isothermal and non-isothermal conditions respectively. The solid line refers to the Lauritzen-Hoffman model identified on experimental data (Equation 10).

Figure 10: Crystallization time for PEKK 70/30 measured from DSC measurement (99% of relative crystallinity) and from thermo-microscopy analyses based on the time for the spherulites to fill the 2D plane of the image.

Figure 11: Time evolution of PEKK 70/30 relative crystallinity for various crystallization temperatures. Comparison of Hillier's model prediction with experimental data from DSC. Contribution of primary and secondary crystallization mechanisms on the isothermal crystallization kinetics as predicted by Hillier's model.

Figure 12: Evolution of w_1 and K_2 [s^{-n_2}] parameters as a function of crystallization temperature. The solid line correspond to the logarithmic line of best fit for each parameter.

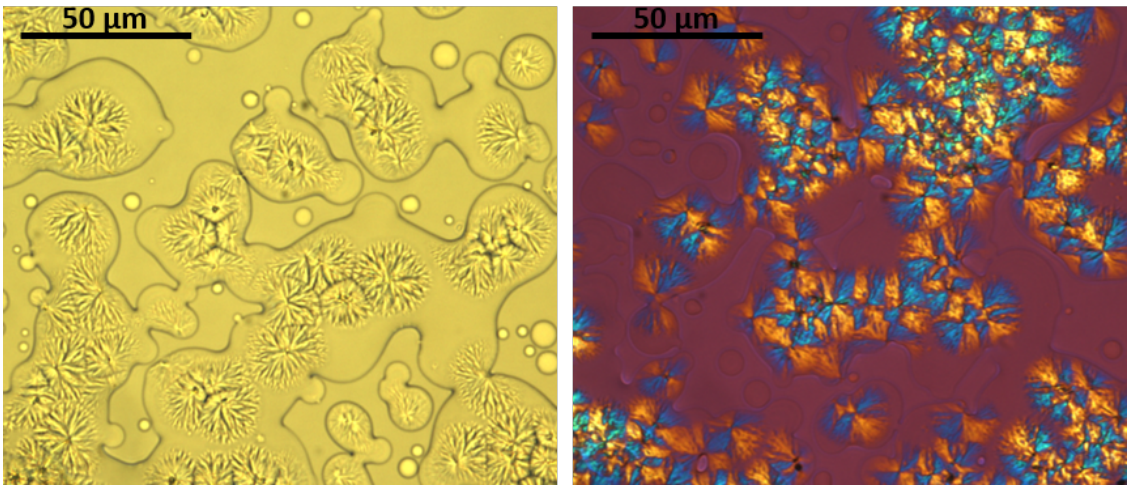

Figure 1
Crystal morphology of PEKK : (left) Lamellae inside spherulites and (right) Maltese cross on spherulites.

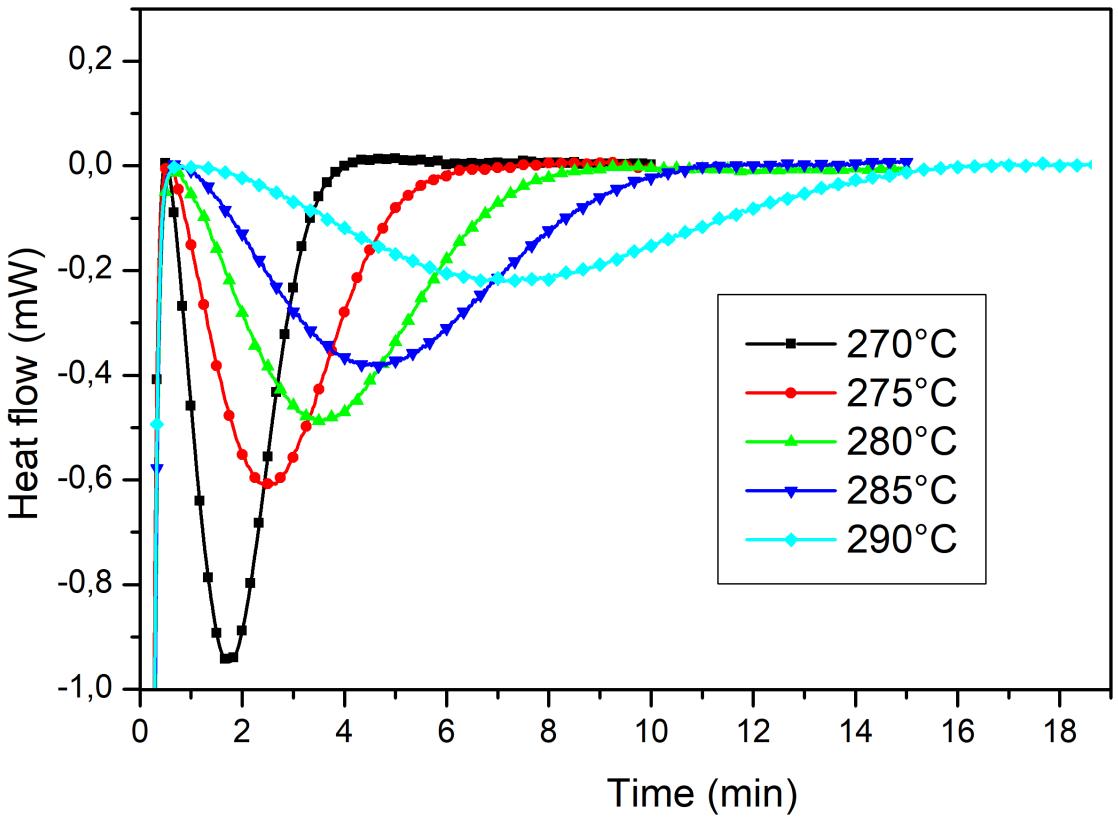

Figure 2
Crystallization exotherms of PEKK 70/30 during isothermal crystallization from the melt.

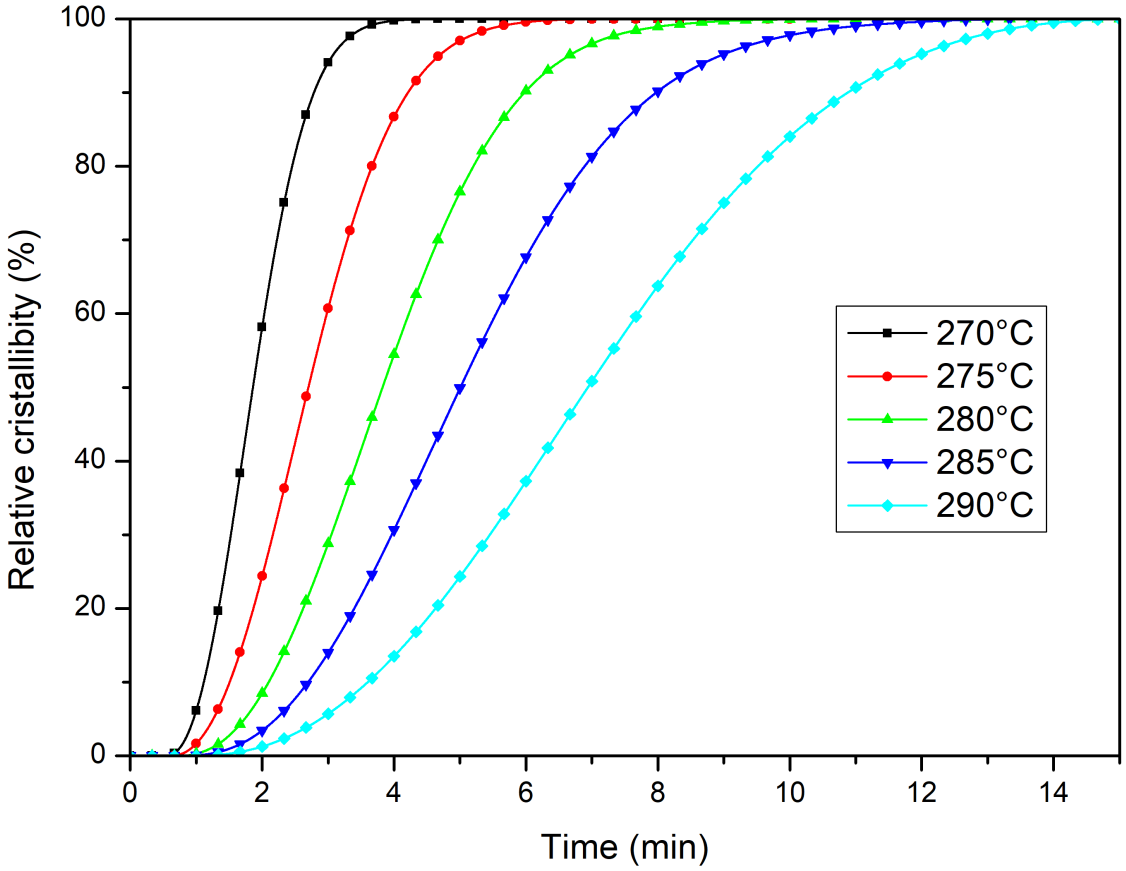

Figure 3
crystallization kinetics of PEKK 70/30 for different isothermal stages.

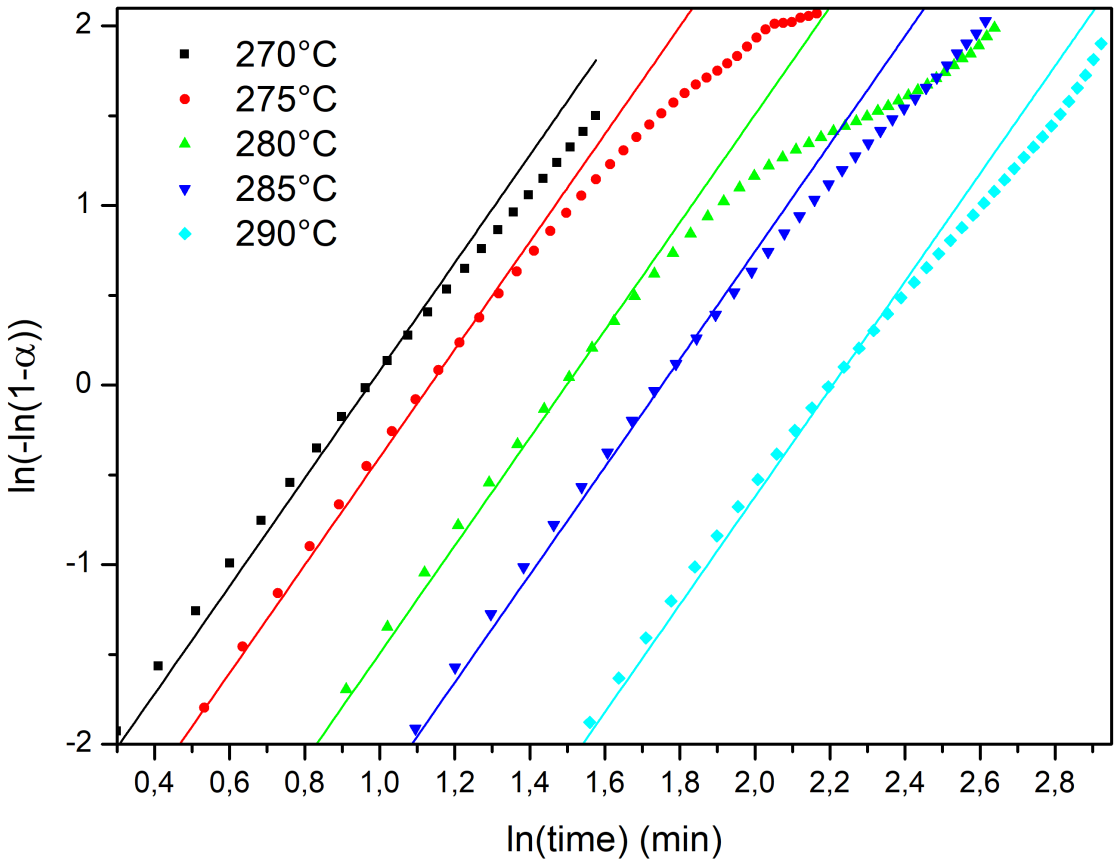

Figure 4
Avrami plot for PEKK 70/30 isothermally crystallized in a DSC between 270°C and 290°C.

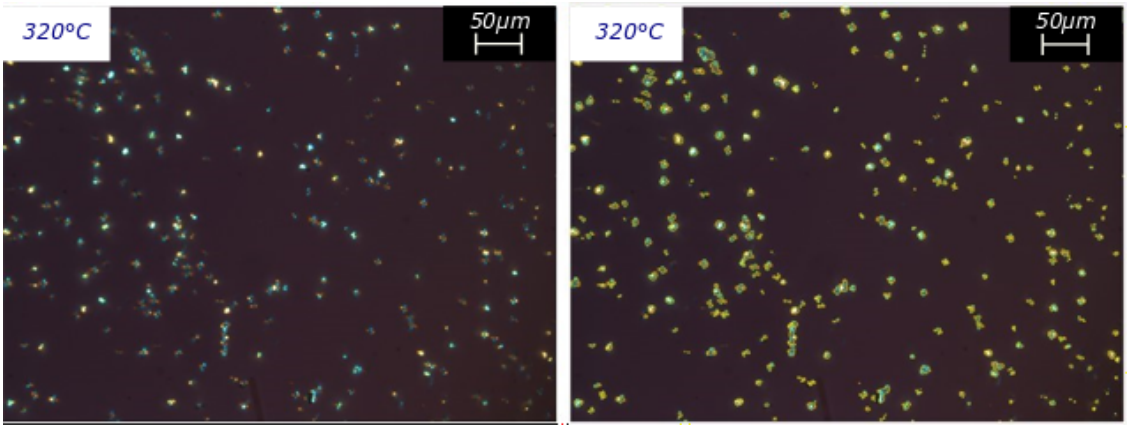

Figure 5
Particles identification in a micrograph thanks to the "particle analysis" module of ImageJ using a threshold of 20 pixels: original image (left) and analyzed image (right).

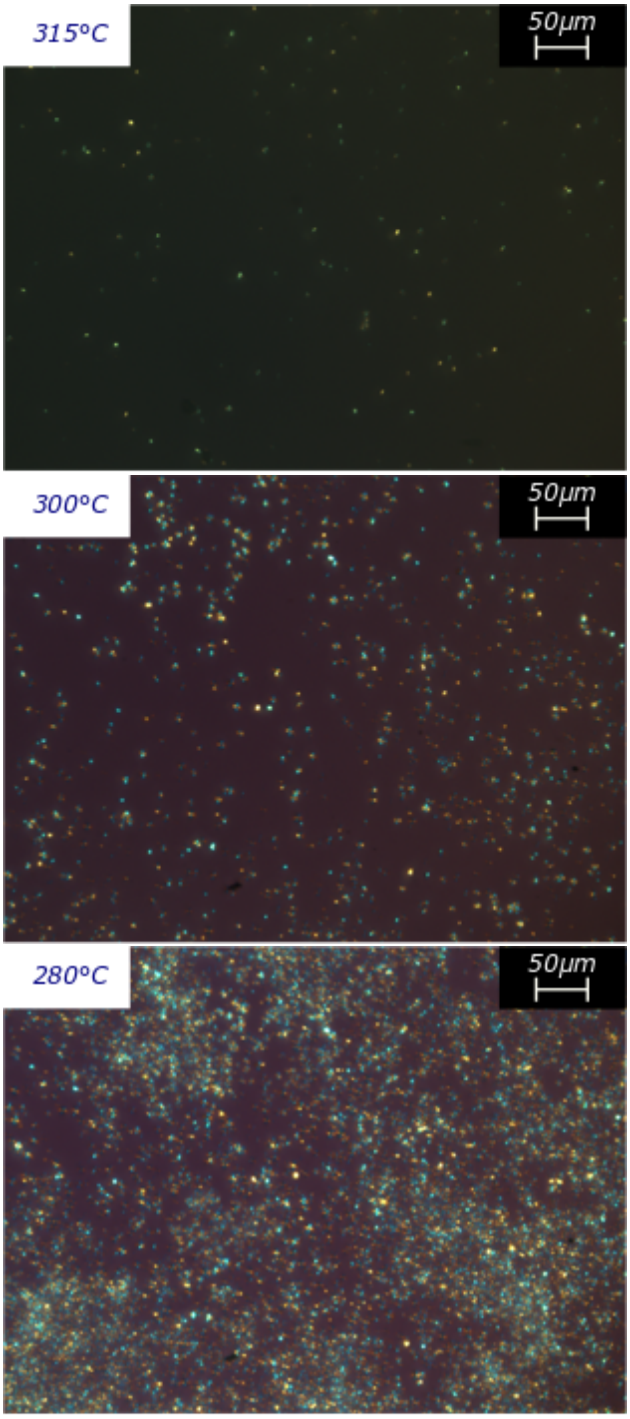
315°C
50µm
300°C
50µm
280°C
50µm

Figure 6
Small spherulites formed in a neat PEKK resin during an isothermal crystallization at 315°C (top left), 300°C (top right) and 280°C (bottom).

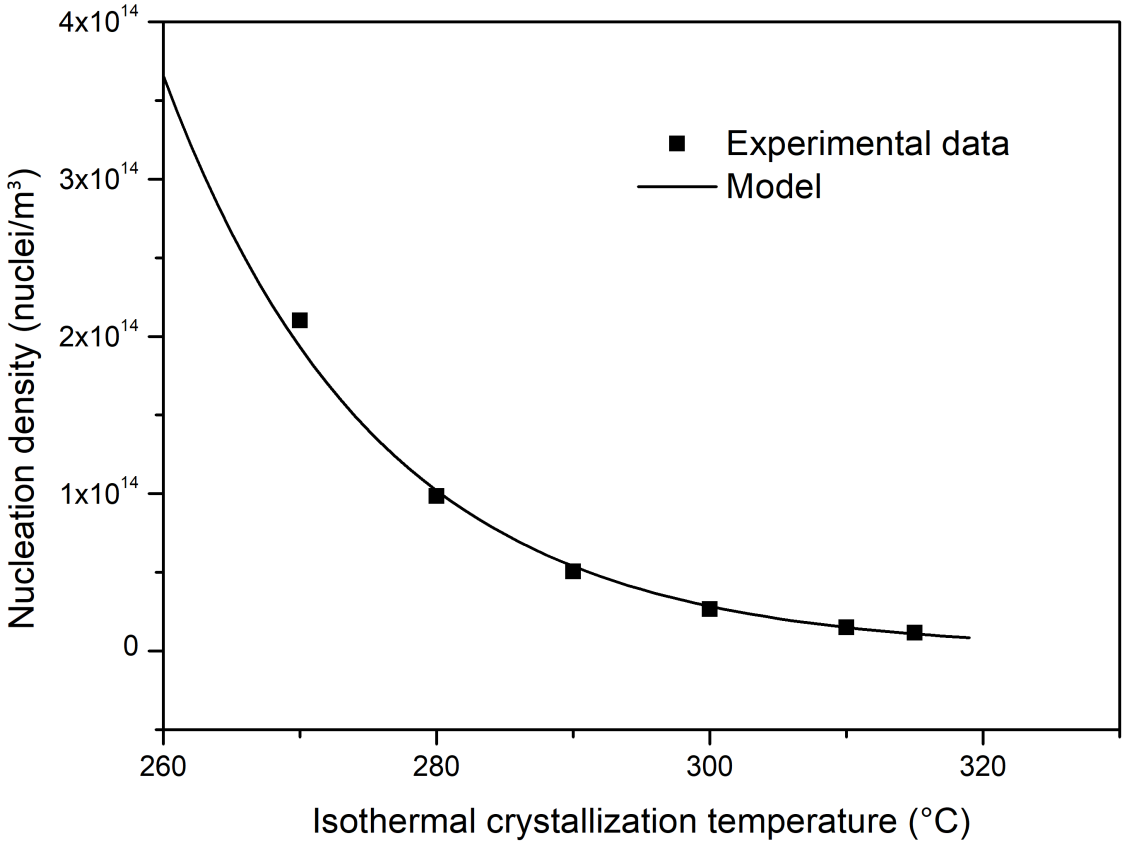

Figure 7
Nucleation density in a neat PEKK resin as a function of isothermal crystallization temperature. Comparison of the simulated and the measured nucleation density for a PEKK 70/30.

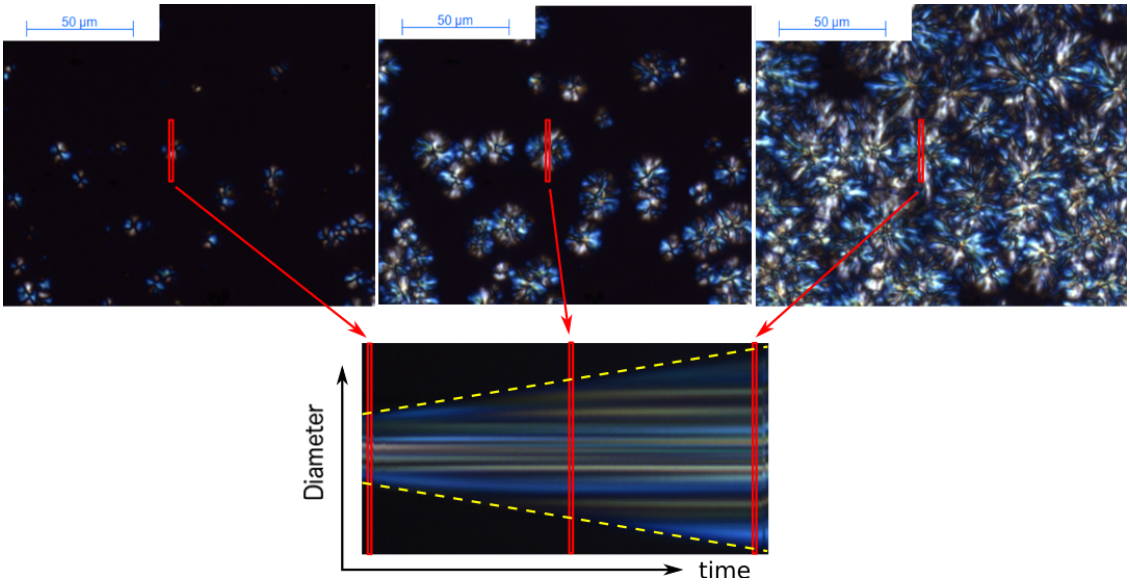

Figure 8
Thermo-microscopy analysis: (top) crystallization of a PEKK 70/30 at 290°C revealed by polarized optical microscopy for three different snapshots (after 75s, 224s and 355s) and (bottom) temporal evolution of the diameter of a spherulite as a function of time.

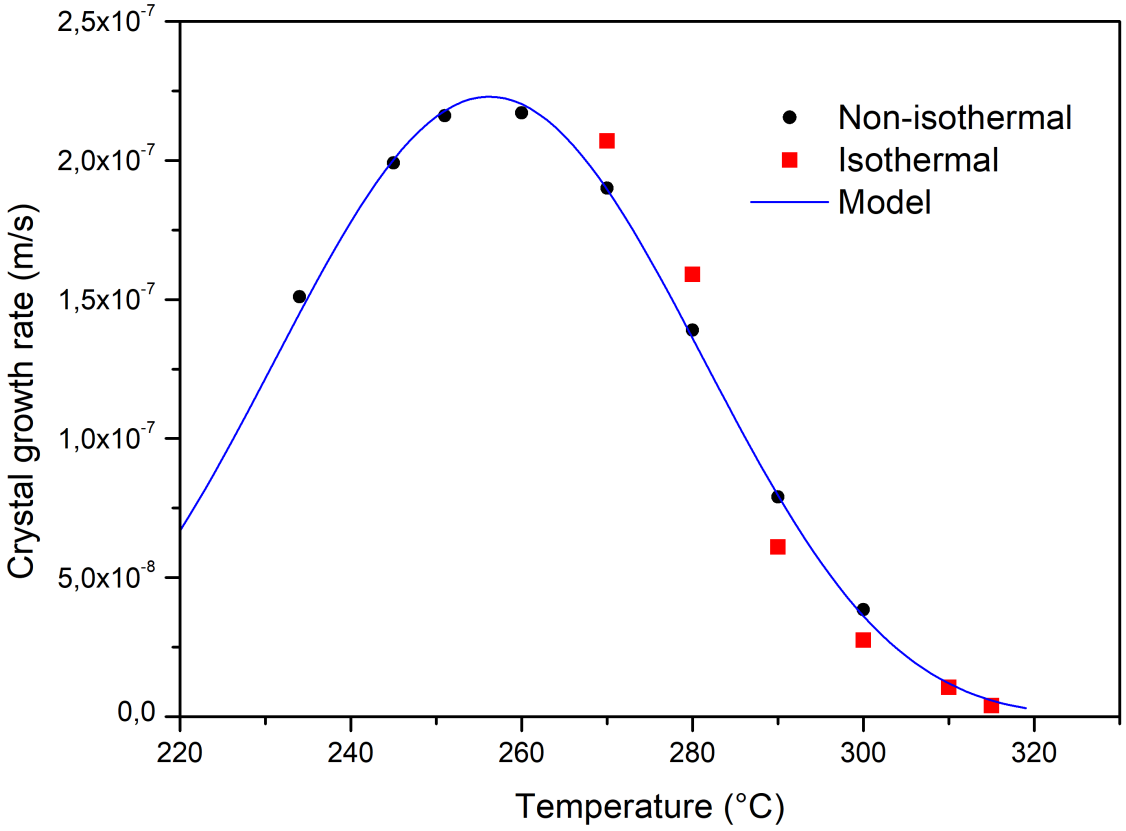

Figure 9
Spherulite growth rate in a PEKK 70/30 resin as a function of isothermal crystallization temperature. The red squares and black circles are experimental data recorded under isothermal and non-isothermal conditions respectively. The solid line refers to the Lauritzen-Hoffman model identified on experimental data (Equation 10).

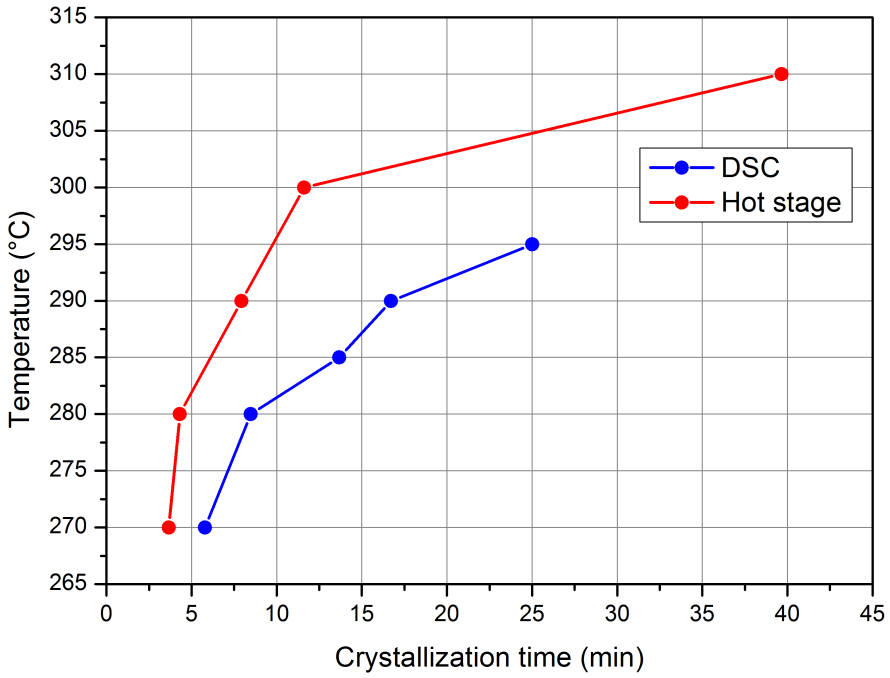

Figure 10
Crystallization time for PEKK 70/30 measured from DSC measurement (99% of relative crystallinity) and from thermo-microscopy analyses based on the time for the spherulites to fill the 2D plane of the image.

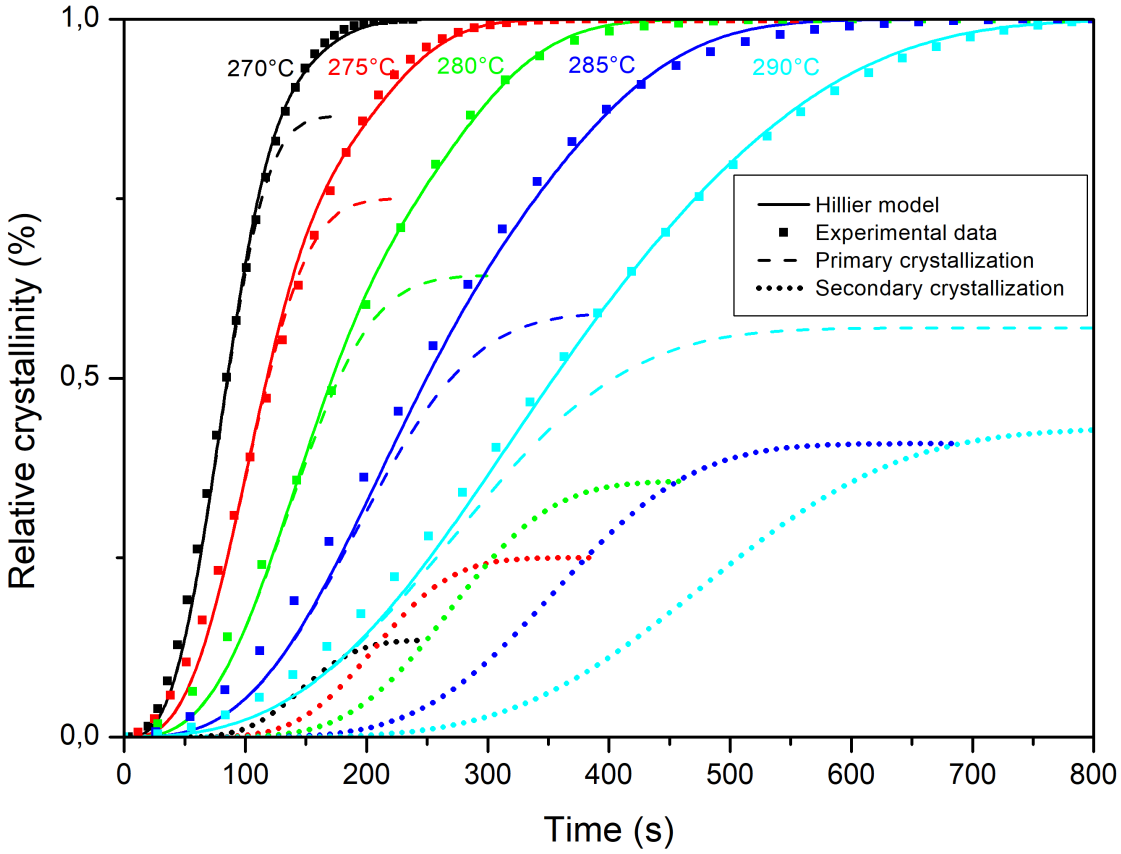

Figure 11
Time evolution of PEKK 70/30 relative crystallinity for various crystallization temperatures. Comparison of Hillier's model prediction with experimental data from DSC. Contribution of primary and secondary crystallization mechanisms on the isothermal crystallization kinetics as predicted by Hillier's model.

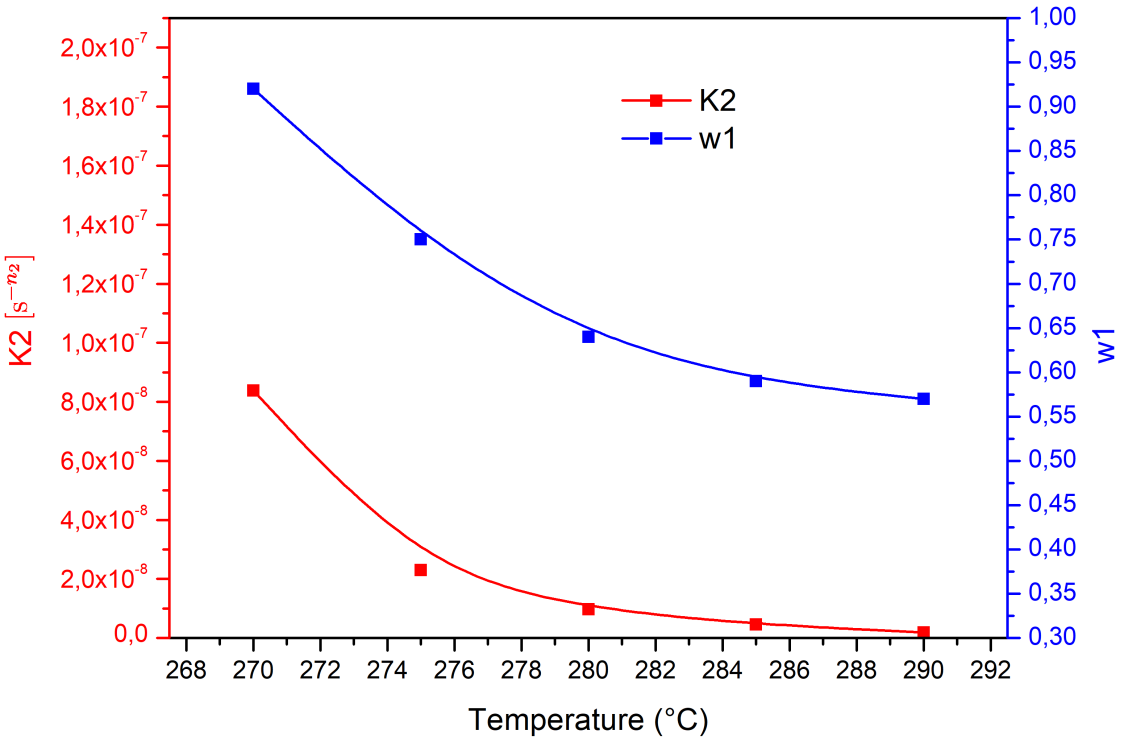

Figure 12
Evolution of w_1 and K_2 $[\mathrm{s}^{-n_2}]$ parameters as a function of crystallization temperature. The solid line correspond to the logarithmic line of best fit for each parameter.